Freezing and Melting of Methyl Chloride in a Single Cylindrical Pore: Anomalous Pore-Size Dependence of Phase-Transition Temperature

Kunimitsu Morishige* and Keizi Kawano

Department of Chemistry, Okayama University of Science, 1-1 Ridai-cho, Okayama 700-0005, Japan

Received: April 8, 1999; In Final Form: June 28, 1999

To study the freezing/melting behavior of a confined CH_3Cl, we performed X-ray diffraction measurements of CH_3Cl confined inside the cylindrical pores of six kinds of siliceous MCM-41 with different pore radii ($R = 1.2-2.9$ nm) as a function of temperature. The pore-size dependence of the phase-transition temperature suddenly changes between $R = 2.5$ and 2.1 nm and between $R = 1.8$ and 1.45 nm. The CH_3Cl confined to the mesopores of $R \geq 1.8$ nm shows a large hysteresis effect between freezing and melting and crystallizes on freezing, while the CH_3Cl confined to the mesopores of $R \leq 1.45$ nm vitrify on cooling. Although the CH_3Cl confined to the mesopores of $R \geq 2.5$ nm freezes into a solid with the same ferroelectric structure as the bulk, the CH_3Cl confined to the mesopores of $R = 1.8$ and 2.1 nm crystallizes into a structure that is different from the bulk. The results are discussed on the basis of a homogeneous nucleation, as well as the effects of finite size on melting point depression and the structure of a confined solid.

I. Introduction

The large surface-area-to-volume ratio of materials confined in porous media provides an opportunity for fundamental studies of the effects of finite size and surface interactions on the phase transitions, structure, and thermodynamic parameters of the confined material. Although the conventional mesoporous materials such as porous Vycor glass[1] and sol−gel glasses[2] have the interconnectivity of a pore network and more or less a pore-size distribution, however, the interpretation of the results obtained on these adsorbents is not straightforward. Recent studies[3−9] show that MCM-41 can be regarded as the most suitable model adsorbent currently available for mesopores. The pores are of cylindrical-like nature, arranged parallel in a honeycomb-type lattice, and their dimensions can be tailored in the range 2−10 nm or more. The absence of pore channel intersections in MCM-41 guarantees that pore-networking effects are negligibly small.

Very recently, we started a series of X-ray diffraction studies on the confined phases in MCM-41 mesoporous adsorbent to examine the liquid−solid phase transitions of a confined phase in a single cylindrical pore.[10,11] The ultimate purpose of this project is to elucidate the long-standing problems of these phase transitions such as the place of nucleation inside pores, the mechanism of phase-transition-temperature lowering, the origin of hysteresis between freezing and melting, and the effects of finite size and surface interactions on the structure of a confined solid. For pore water, the melting point depression was inversely proportional to the effective pore size[11,12] and the hysteresis effect depended markedly on the size of the pores.[11] This strongly suggest that the nucleation occurs in the middle of the pores (homogeneous nucleation) and that the hysteresis is from the presence of a kinetic barrier to crystallization of water confined to the mesopores. The X-ray diffraction patterns of the frozen water in the mesopores were best fit by a mixture of crystalline structures between stable hexagonal ice and metastable cubic ice,[13] suggesting that their structures reflect density fluctuations essential to the formation of a critical nucleus rather than the surface interactions with pore wall or the kinetic factor due to deep supercooling. Before drawing a definite conclusion to these problems, however, systematic and extensive studies on other molecules will be needed.

Recent work by Gay et al.[14] has shown that methyl chloride freezes into a non-close-packed, ferroelectric structure stabilized by the dipole moment, although in general dipolar interactions rarely lead to structures that are in conflict with the requirements of efficient lattice packing. On the other hand, the Landau phenomenological theory[15] has shown that the spontaneous polarization in ferroelectric particles decreases with decreasing particle size and eventually disappears; i.e., a size-driven phase transition takes place. The purpose of the present study is to address some of the above-mentioned problems by examining the freezing and melting behavior, as well as the structure of the frozen solid, of methyl chloride confined in MCM-41 adsorbents with well-defined pore radii by means of X-ray diffraction.

II. Experimental Section

Sample preparations and characterization have been described in a previous paper.[11] Six kinds of MCM-41 adsorbents with pore radii of 1.2, 1.45, 1.8, 2.1, 2.5, and 2.9 nm were used in the present experiments.

The experimental apparatus of X-ray diffraction for freezing/melting measurements has been also described in detail elsewhere.[16] The measurements were carried out with Mo Kα radiation in s symmetrical transmission geometry. The rotating anode source was operated at 50 kV and 200 mA. A MCM-41 self-supporting disk (∼0.02 g) of 12 mm diameter was attached to a cold head of a He closed-cycle refrigerator. After prolonged evacuation at room temperature, the substrate was cooled and then the background spectra were measured at two temperatures of 120 and 40 K. Adsorption isotherms of methyl chloride on MCM-41 inside the X-ray cryostat were measured at 180 K. In

* To whom correspondence should be addressed. E-mail: morishi@chem.ous.ac.jp. Fax:086-254-2891.

10.1021/jp991177m CCC: $18.00
Published on Web 08/27/1999

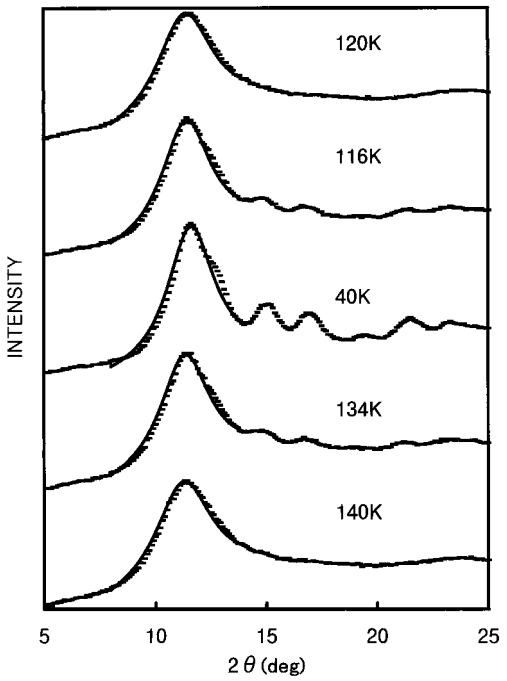

Figure 1. Change of X-ray diffraction pattern of CH_3Cl confined to the mesopores of $R = 2.5$ nm upon cooling and warming. The top three patterns and the bottom two patterns are measured upon cooling and warming, respectively. Solid lines are Lorentzian fits to the data.

X-ray measurements, the adsorbed amounts were kept slightly below the saturation to avoid contamination in diffraction pattern from the bulk phase formed outside the mesopores. The substrate was then cooled to a desired temperature, and the spectrum was remeasured. After correction for attenuation due to substrate and adsorbed gas, the diffraction pattern of a confined phase was obtained by subtraction of data for charged and empty substrates.

III. Results

The adsorption isotherm for MCM-41 with pore radius (R) of 1.2 nm was of type I, while those for MCM-41 with larger R were of type IV. The step due to capillary condensation shifted into higher pressure with increasing R.

Figure 1 shows some of the diffraction patterns from the CH_3Cl confined to the cylindrical pores of MCM-41 with R of 2.5 nm when the temperature was successively lowered and then when the temperature was successively increased. One run took about 80 min. On cooling, one obtains still pure liquid scattering at 120 K, well below the bulk melting point of 175.6 K. As the temperature is lowered through 116 K, there is a rather abrupt change in the diffraction pattern from liquid to solid form. The transformation was almost completed at 112 K. A further decrease in temperature up to 40 K did not result in an appreciable change in the line shape except for a slight increase in the peak height due to the Debye−Waller factor and intensification of a shoulder peak around $2\theta = 12.5°$. When the substrate was warmed, a profound hysteresis in freezing and melting temperatures was observed. At 134 K, the diffraction pattern still preserves the solid form. The hysteresis loop between freezing and melting amounts to ~18 K in width.

To obtain accurate peak parameters, the observed peak profile was fitted to a Lorentzian line shape with a linearly changing background in a limited 2θ range.[17] The solid lines in Figure 1 are fits to a Lorentzian line shape. Figure 2 shows the peak positions and widths (full width at half-maximum (fwhm))

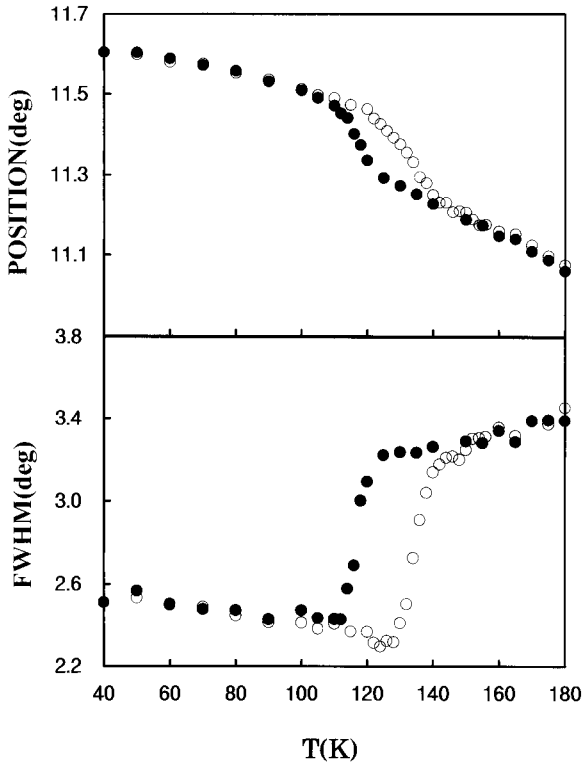

Figure 2. Peak position and width (fwhm) as a function of temperature for CH_3Cl confined to the mesopores of $R = 2.5$ nm. Open and closed symbols denote warming and cooling processes, respectively.

obtained from Lorentzian fits to the main peaks as a function of temperature for the CH_3Cl confined to the mesopores of $R = 2.5$ nm. The variation of the peak width as a function of temperature shows that freezing (T_f) and melting points (T_m) of the confined CH_3Cl in the mesopores of $R = 2.5$ nm are 116 and 134 K, respectively. In the region of the solid phase, the peak width obtained from the fitting increased with decreasing temperature. This comes from the intensification of the shoulder peak around $2\theta = 12.5°$ rather than the broadening of the main peak. Similarly, premelting of the confined CH_3Cl is accompanied by weakening of the shoulder peak, as is revealed by a slight decrease in the peak width obtained from fitting just before melting. When the substrate was cooled, the peak position shifted steeply into a higher scattering angle, which suggests a rapid increase in density of the CH_3Cl confined to the mesopores. Freezing of the CH_3Cl results in the rapid increase in peak position, which corresponds to the formation of crystalline solid. When the confined solid was warmed, the peak position shifted remarkably into a lower angle just before the beginning of melting at 130 K, indicating the occurrence of premelting.

It is well-known that when liquids and solids are restricted in mesopores, their freezing and melting temperatures will be depressed and the melting point depression is almost inversely proportional to the pore size.[18−22] For the CH_3Cl confined to the cylindrical pores of MCM-41, however, such a pore-size dependence of the phase-transition temperature was violated in the mesopores of $R \leq 2.1$ nm. Figure 3 shows the peak positions and widths obtained from Lorentzian fits to the main peak as a function of temperature for the CH_3Cl confined to the mesopores of $R = 2.1$ nm. The variation of the peak width shows that T_f and T_m of the CH_3Cl confined to the mesopores of $R = 2.1$ nm are ~88 and 115 K, respectively. Despite the slight decrease in pore size from $R = 2.5$ to 2.1 nm, both the transition temperatures lowered significantly. The temperature dependence

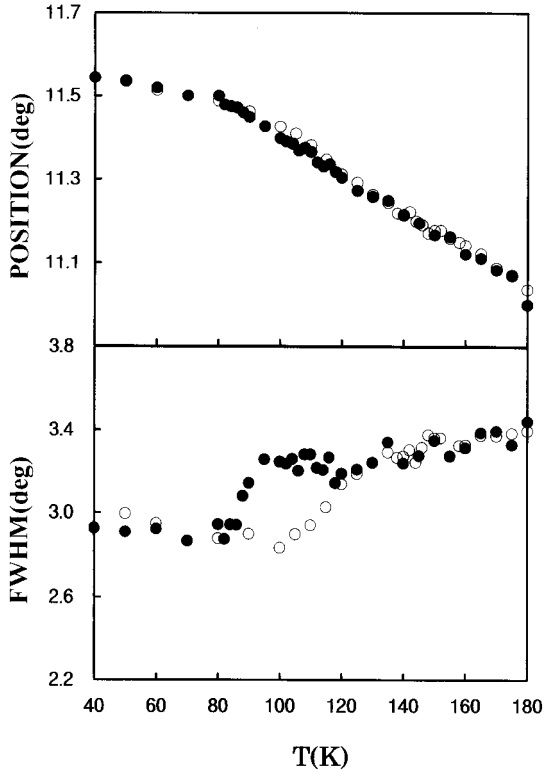

Figure 3. Peak position and width (fwhm) as a function of temperature for CH_3Cl confined to the mesopores of $R = 2.1$ nm. Open and closed symbols denote warming and cooling processes, respectively.

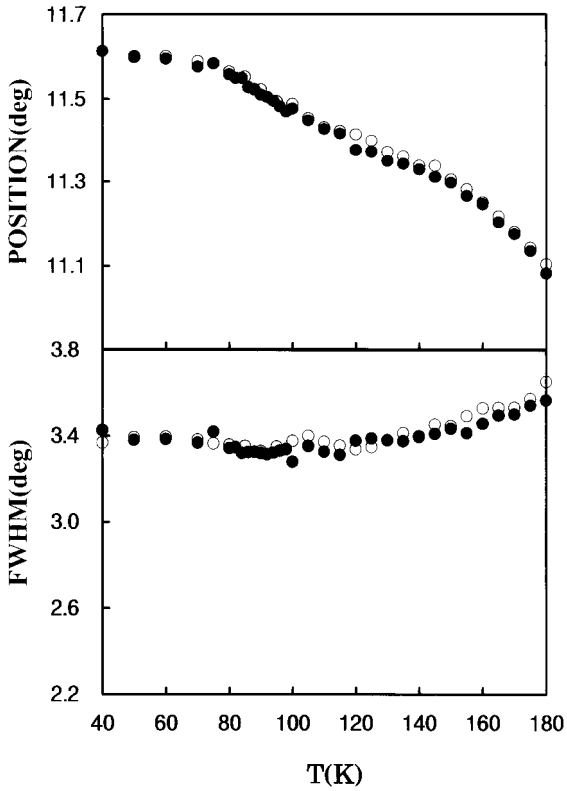

Figure 4. Peak position and width (fwhm) as a function of temperature for CH_3Cl confined to the mesopores of $R = 1.45$ nm. Open and closed symbols denote warming and cooling processes, respectively.

of the peak position changed around 85 K, regardless of the processes of cooling and warming. This favorably corresponds to T_f of the confined CH_3Cl, while this temperature is below T_m by ~30 K. A further reduction of pore size up to $R = 1.45$ nm led to the appearance of a glassy phase. Figure 4 shows the peak positions and widths obtained from Lorentzian fits to the main peak as a function of temperature for the CH_3Cl confined to the mesopores of $R = 1.45$ nm. When the sample was cooled, the peak width slightly decreased in the temperature region 180−100 K and remained almost constant and relatively large below 100 K. The temperature dependence of the peak position changed around 75 K, regardless of the processes of cooling and warming. This suggests that the glass-transition temperature of the CH_3Cl confined to the mesopores of $R = 1.45$ nm is ~75 K. Table 1 summarizes the freezing/melting temperatures of the CH_3Cl confined in MCM-41.

TABLE 1: Freezing (T_f), Melting (T_m), and Glass-Transition (T_g) Temperatures of CH_3Cl Confined in MCM-41

R (nm)	T_f (K)	T_m (K)	T_g (K)
2.9	120	138	
2.5	116	134	
2.1	88	115	
1.8	88	112	
1.45			~75
1.2			~70

IV. Discussion

A. Structure of Confined Solid. Figure 5 shows the X-ray diffraction patterns of the frozen CH_3Cl confined to the cylindrical mesopores of MCM-41 as a function of pore size at 40 K. These three patterns are different from each other. The diffraction pattern for $R = 2.5$ nm is crystalline, while that for $R = 1.45$ nm is amorphous. The diffraction pattern for $R = 2.1$ nm seems to be a superposition of crystalline and amorphous patterns. We investigated the structures of the confined solid CH_3Cl by comparing the observed diffraction pattern with that simulated using the Debye formula[23] appropriate to the calculation of the powder diffraction pattern of small particles. We have considered only carbon and chlorine atoms in the simulation and neglected to include the incoherent scattering. The Debye formula automatically averages over the different cluster orientations in the sample. The structure of the bulk crystal, which has the symmetry of the space group *Cmc*21, is noncentrosymmetric with a basis of two molecules.[24] The Bravais lattice is base-centered orthorhombic with four molecules per unit cell, and the molecules are stacked in an AB fashion with molecules in alternating layers differing by a C_2 rotation about the axis perpendicular to the layers. The lattice constants are $a = 6.495$, $b = 5.139$, and $c = 7.523$ Å at 148 K. The coordinates of the atoms in the simulated clusters were obtained by systematically generating atomic positions for a crystalline cube, arbitrarily choosing a point in the center of this cube as the origin, and only retaining those atoms that fall within a sphere of the chosen radius. A root-mean-square fluctuation of all the atoms at 40 K was fixed at a value of 0.15 Å, while that of the bulk crystal was 0.19 Å at 148 K.

The diffraction pattern of the frozen CH_3Cl within the cylindrical mesopores of $R = 2.5$ nm is compared with the simulated spectrum of spheres with the same structure as the bulk and with a nominal radius of 2.0 nm in Figure 5. Here, the assumption of a spherical particle does not necessarily mean that the confined solid virtually takes a spherical form within the cylindrical mesopores of MCM-41. The pattern for a powder of the cylindrical microcrystals grown in different lattice directions may be reproduced by the diffraction pattern calculated for a spherical microcrystal. The total number of molecules in a 2.0 nm radius sphere is ~500. Except for the shoulder peak around $2\theta = 12.5°$ and a diffuse background, all the features

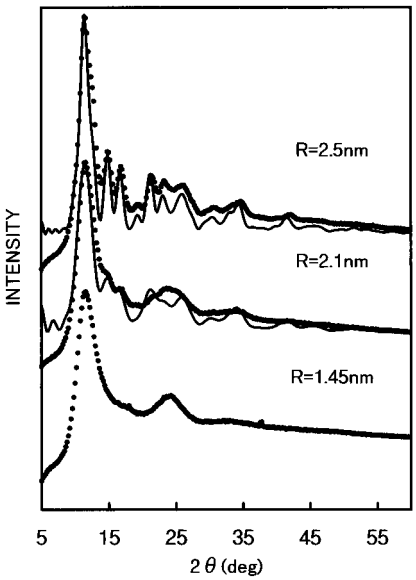

Figure 5. X-ray diffraction patterns of CH_3Cl confined within MCM-41 as a function of pore size at 40 K. Solid lines denote the simulated patterns of the spheres with the bulk structure and with $l_{ij} = 0.15$ Å.

in the experimental diffraction pattern are well reproduced in simulation. The crystalline size smaller than the pore size suggests the presence of an amorphous layer adjacent to the pore wall. Molecular motion of the first monolayer adjacent to the pore wall is known to be drastically different from that of the liquid at the center of the pore.[2,25−27] This layer exhibits freezing behavior different from that of the liquid in the middle of the pore.[12,28,29] The interfacial phase confined between the microcrystal in the middle of the pores and the amorphous pore wall may contribute to the diffuse scattering component. Although the inclusion of a small amount of stacking faults by reversing the molecular axis slightly improved the fit between the experimental and simulated spectrum, the shoulder peak at $2\theta = 12.5°$ was never reproduced. The present analysis neglects the molecule/silica correlations. Presumably this cross-correlation term will contribute to the diffuse scattering component, too.

The reduction in pore size from $R = 2.5$ to 2.1 nm results in a severe line broadening in the diffraction pattern of the frozen solid, suggesting a sudden decrease in crystal size of the solid formed by freezing. This gives partly a good account of the large depression in freezing and melting points of the phase confined to the mesopores of $R = 2.1$ nm. As Figure 5 shows, however, reduction in particle size under the assumption of the same structure as the bulk does not reproduce well the diffraction patterns of the frozen CH_3Cl within the mesopores of $R = 2.1$ nm. The simulated spectrum was obtained on spheres with the same structure as the bulk and with a nominal radius of 1.2 nm. The sphere contains ∼110 molecules. Smaller pore sizes may result in an increase in contribution of the interfacial phase adjacent to the pore wall, as well as the molecule/silica correlations, on the diffraction pattern observed. Although before drawing the definite conclusion that the total analysis based on the considerations of all these effects is required, it is suggested that the CH_3Cl confined to the mesopores of $R = 1.8$ and 2.1 nm crystallizes into a structure different from the bulk structure.

B. Anomalous Pore-Size Dependence of Phase-Transition Temperatures. The melting point of bulk CH_3Cl is 175.6 K, and the lowest temperature to which the bulk liquid could be supercooled is 120 ± 1.5 K.[30] As Figure 6 shows, the pore-size dependence of the phase-transition temperature suddenly

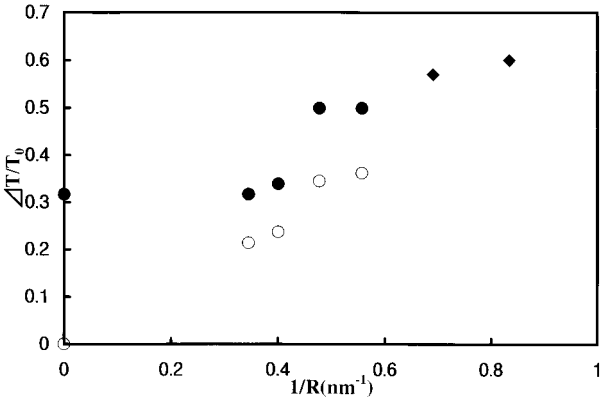

Figure 6. Melting and freezing point depressions against $1/R$. Open and closed circles denote melting and freezing point depressions, respectively. Closed diamond denotes glass-transition temperatures of phases confined to smaller pores.

changes between $R = 2.5$ and 2.1 nm and between $R = 1.8$ and 1.45 nm. Above $R = 2.5$ nm the melting point seems to be almost inversely proportional to R, as is usually observed in confined phases. Below $R = 2.1$ nm, this pore-size dependence is no longer held. In contrast to the expectation from the inverse correlation of the transition temperatures and R, the freezing and melting temperatures changed significantly between $R = 2.5$ and 2.1 nm and the transition temperatures of the CH_3Cl confined to the mesopores of $R = 2.1$ and 1.8 nm were almost independent of R. The CH_3Cl confined to the mesopores of $R \geq 1.8$ nm crystallizes on freezing, and the hysteresis effect between freezing and melting amounts to ∼20 K, while the CH_3Cl confined to the mesopores of $R \leq 1.45$ nm vitrifies on cooling.

Confinement of liquids to small pores results in a finite-size-related shifting of the phase diagram (thermodynamical supercooling).[18−22] On a laboratory time scale liquids can be further supercooled below the thermodynamic freezing transition because of the presence of a kinetic barrier to crystallization (genuine and dynamical supercooling).[31−34] In homogeneous nucleation, this barrier can be reduced only through deep supercooling. It is well-known, however, that bulk liquids cannot be supercooled below the particular temperatures where the thermal energy becomes comparable to the reduced kinetic barrier.[35,36] When the properties of liquids confined to the mesopores are similar to those of bulk liquids, the confined liquids would also be impossible to supercool below their characteristic temperatures by only dynamical supercooling because of the low kinetic barrier to homogeneous nucleation. In other words, the liquids undercooled due to thermodynamical supercooling below their characteristic temperatures would not show any hysteresis effects between freezing and melting. The amount of the thermodynamical supercooling may be estimated according to the Gibbs−Thomson or related equation. The freezing/melting behavior of the water in the middle of the mesopores of porous silicas was well accounted for by such an idea.[11] The freezing and melting point depressions of the CH_3Cl confined to the mesopores of $R \geq 2.5$ nm seem to be compatible with the expectations from the dynamical supercooling and from the thermodynamical supercooling, respectively. In the homogeneous nucleation of the CH_3Cl confined to the mesopores of MCM-41, several critical nuclei spontaneously generate in the single cylindrical pore. The length of the cylindrical pores of MCM-41 attains ∼40 nm.[37] If only one nucleus were generated in the single pore, the resulting

microcrystal grown within the pore would give a diffraction pattern with sharper peaks expected from its larger crystallite size.

Contrary to the expectation from the homogeneous nucleation, the CH_3Cl confined to the mesopores of $R = 1.8$ and 2.1 nm was undercooled below the characteristic temperature (120 K) of the bulk liquid and yet showed a large hysteresis effect between freezing and melting. This does not necessarily mean, however, that the hysteresis effect is not due to the presence of a kinetic barrier to crystallization. When the CH_3Cl confined to the mesopores of $R = 1.8$ and 2.1 nm crystallizes into a structure different from that of the bulk, the amount of supercooling for the bulk liquid quoted above, as well as the bulk melting point itself, is not justified for the CH_3Cl confined to these mesopores. The melting point depressions observed for both the mesopores of $R = 1.8$ and 2.1 nm deviate significantly from the inverse correlation expected between the transition temperatures and R. This also supports the idea that the CH_3Cl confined to these mesopores crystallizes into a new structure.

C. Effect of Finite Size on the Structure of a Confined Solid. On cooling, the CH_3Cl confined to the cylindrical mesopores of MCM-41 solidifies into different structures depending on the pore size: a bulk structure for $R \geq 2.5$ nm, a crystalline structure different from the ferroelectric bulk structure for 1.8 nm $\leq R \leq$ 2.1 nm, and a glassy state for $R \leq$ 1.45 nm. The Landau phenomenological theory[15] has shown that for ferroelectric particles a size-driven ferroelectric/paraelectric phase transition occurs and that the ferroelectric critical size at which the phase transition takes place is the smallest size that can sustain ferroelectricity. Although the structure of the frozen CH_3Cl confined to the mesopores of $R = 1.8$ and 2.1 nm is unknown, the ferroelectric critical size of a solid CH_3Cl may be near 2.1 nm.

On cooling, water[11] crystallizes in the small pores of $R =$ 1.2 nm while several molecules such as D_2,[8] CH_4,[8] and N_2[38] do not crystallize even within the pores of $R \approx 2.0$ nm. Krypton crystallizes in the mesopores of $R = 2.0$ nm[8,38] and does not crystallize in the smaller mesopores of $R = 1.45$ nm.[39] The amount of the gap between the normal freezing point and the glass-transition temperature in each molecule may be related to the behavior difference between these confined phases. The larger gap between these two temperatures would give more chance for the molecules to crystallize in the course of freezing, while less gap would lead to freezing of a supercooled state (a glassy state) owing to a large freezing point depression due to the Gibbs−Thomson effect. Although we do not know T_g of CH_3Cl, vitrification of the CH_3Cl confined to the mesopores of $R \leq 1.45$ nm may occur through such a mechanism. On the other hand, Sokol et al.[40] have thought that near the pore walls the molecules form an amorphous structure to accommodate the complex wall geometry as best they can and then this amorphous structure propagates into the interior of the pores by a healing length depending on the ratio of the wall/liquid interactions. If the appearance of the amorphous CH_3Cl solid within the mesopores of $R \leq 1.45$ nm was due to the effect of surface interactions with the pore wall, the healing length of CH_3Cl with the pore wall of siliceous MCM-41 would attain $\sim$1.45 nm at least. This implies that the diffraction patterns of the frozen CH_3Cl confined to the pores of $R \geq 1.8$ nm could be dominated by an amorphous component larger than actually observed.

References and Notes

(1) Levitz, P.; Ehret, G.; Sinha, S. K.; Drake, J. M. *J. Chem. Phys.* **1991**, *95*, 6151.
(2) Liu, G.; Li, Y.; Jonas, J. *J. Chem. Phys.* **1991**, *95*, 6892.
(3) Kresge, C. T.; Leonowicz, M. E.; Roth, W. J.; Vartuli, J. C.; Beck, J. S. *Nature (London)* **1992**, *359*, 710.
(4) Branton, P. J.; Hall, P. G.; Sing, K. S. W. *J. Chem. Soc., Chem. Commun.* **1993**, 1257.
(5) Rathousky, J.; Zutal, A.; Franke, O.; Shulz-Ekloff, G. *J. Chem. Soc., Faraday Trans.* **1995**, *91*, 937.
(6) Ravikovitch, P. I.; O'Domhnail, S. C.; Neimark, A. V.; Schuth, F.; Unger, K. K. *Langmuir* **1995**, *11*, 4765.
(7) Hansen, E. W.; Stocker, M.; Schmidt, R. *J. Phys. Chem.* **1996**, *100*, 2195.
(8) Llewellyn, P. L.; Grillet, Y.; Rouquerol, J.; Martin, C.; Coulomb, J.-P. *Surf. Sci.* **1996**, *352*−*354*, 468.
(9) Morishige, K.; Shikimi, M. *J. Chem. Phys.* **1998**, *108*, 7821.
(10) Morishige, K.; Nobuoka, K. *J. Chem. Phys.* **1997**, *107*, 6965.
(11) Morishige, K.; Kawano, K. *J. Chem. Phys.* **1999**, *110*, 4867.
(12) Schmidt, R.; Hansen, E. W.; Stocker, M.; Akporiaye, D.; Ellestad, O. H. *J. Am. Chem. Soc.* **1995**, *117*, 4049.
(13) Morishige, K.; Kawano, K. To be published.
(14) Gay, S.; Beale, P. D.; Rainwater, J. C. *J. Chem. Phys.* **1998**, *109*, 6820.
(15) Zhong, W. L.; Wang, Y. G.; Zhang, P. L.; Qu, B. D. *Phys. Rev. B* **1994**, *50*, 698.
(16) Morishige, K.; Inoue, K.; Imai, K. *Langmuir* **1996**, *12*, 4889.
(17) Awaya, T. *Nucl. Instrum. Methods* **1979**, *165*, 317.
(18) Rennie, G. K.; Clifford, J. *J. Chem. Soc., Faraday Trans. 1* **1977**, *73*, 680.
(19) Jackson, C. L.; McKenna, G. B. *J. Chem. Phys.* **1990**, *93*, 9002.
(20) Awschalow, D. D.; Warnock, J. *Phys. Rev. B* **1987**, *35*, 6779.
(21) Unruh, K. M.; Huber, T. E.; Huber, C. A. *Phys. Rev. B* **1993**, *48*, 9021.
(22) Hansen, E. W.; Gran, H. C.; Sellevold, E. J. *J. Phys. Chem. B* **1997**, *101*, 7027.
(23) Morozumi, C.; Ritter, M. L. *Acta Crystallogr.* **1953**, *6*, 588.
(24) Burbank, R. D. *J. Am. Chem. Soc.* **1953**, *75*, 1211.
(25) Nikiel, L.; Hopkins, B.; Zerda, T. W. *J. Phys. Chem.* **1990**, *94*, 7458.
(26) Korb, J.-P.; Malier, L.; Cros, F.; Xu, S.; Jonas, J. *Phys. Rev. Lett.* **1996**, *77*, 2312.
(27) Loughnane, B. J.; Fourkas, J. T. *J. Phys. Chem. B* **1998**, *102*, 10288.
(28) Stapf, S.; Kimmich, R. *J. Chem. Phys.* **1995**, *103*, 2247.
(29) Zavada, T.; Kimmich, R. *J. Chem. Phys.* **1998**, *109*, 6929.
(30) Thomas, D. G.; Staveley, L. A. K. *J. Chem. Soc.* **1952**, 4569.
(31) Shimoda, M.; Mizusaki, T.; Hirai, M.; Eguchi, K. J. *Low Temp. Phys.* **1986**, *64*, 285.
(32) Vanfleet, R. R.; Mochel, J. M. *Surf. Sci.* **1995**, *341*, 40.
(33) Sullivan, N. S.; Rall, M.; Brison, J. P. J. *Low Temp. Phys.* **1995**, *98*, 383.
(34) Borisov, B. F.; Charnaya, E.V.; Plotnikov, P. G.; Hoffmann, W.-D.; Michel, D.; Kumzerov, Yu. A.; Tien, C.; Wur, C.-S. *Phys. Rev. B* **1998**, *58*, 5329.
(35) Turnbull, D. *J. Appl. Phys.* **1950**, *21*, 1022.
(36) Jackson, K. A. *Ind. Eng. Chem.***1965**, *57*, 29.
(37) Mokaya, R.; Zhou, W.; Jones, W. J. *Chem. Soc., Chem. Commun.* **1999**, 51.
(38) Coulomb, J. P.; Martin, C.; Grillet, Y.; Llewellyn, P. L.; Andre, G. In *Mesoporous Molecular Sieves*; Bonneviot, L., Beland, F., Danumah, C., Giasson, S., Kaleaguine, S., Eds.; Studies in Surface Science and Catalysis 117; Elsevier: Amsterdam, 1998; p 309.
(39) Morishige, K.; Kawano, K. To be published.
(40) Sokol, P. E.; Ma, W. J.; Herwig, K. W.; Snow, W. H.; Wang, Y.; Koplik, J.; Banavar, J. R. *Appl. Phys. Lett.* **1992**, *61*, 777.